Mon. Not. R. Astron. Soc. **355,** 20–30 (2004) doi:10.1111/j.1365-2966.2004.08278.x

Near-infrared *K*-band imaging of a sample of ultra-steep-spectrum radio sources selected at 74 MHz

Matt J. Jarvis,[1⋆] Maria J. Cruz,[1] Aaron S. Cohen,[2] Huub J. A. Röttgering[3] and Namir E. Kassim[2]

[1]*Astrophysics, Department of Physics, Keble Road, Oxford OX1 3RH*
[2]*Naval Research Laboratory, Code 7213, Washington, DC 20375, USA*
[3]*Leiden University, Sterrewacht, Oort Gebouw, PO Box 9513, 2300 RA Leiden, the Netherlands*

Accepted 2004 August 3. Received 2004 July 1; in original form 2004 May 26

ABSTRACT

In this paper we present near-infrared *K*-band imaging of a sample of ultra-steep-spectrum (USS) radio sources selected at 74 MHz. The dual selection criteria of low frequency and USS mean that we should be sensitive to the highest-redshift ($z > 5$) radio galaxies. We have obtained *K*-band magnitudes for all of the objects in our sample of 26 and discuss the properties of each.

There is a pronounced bias in this sample towards fainter magnitudes and thus higher redshifts when compared to complete unfiltered samples such as the 7CRS of Willott et al., implying that the steep-spectrum technique is still viable at 74 MHz. However, there are more bright ($K < 17$) sources in the 74-MHz sample than in a similar sample selected at 151 MHz, namely 6C*. This is principally due to the additional selection criterion of a small angular size for the radio sources in 6C*; four of the six sources in the 74-MHz USS sample with $K < 17$ have angular sizes >15 arcsec (the angular size cut-off of 6C*).

We find that the distribution of *K*-band magnitudes from a sample selected at 74 MHz is statistically indistinguishable from the 6C* sample, when similar angular size filtering is applied to the 74-MHz sample.

Key words: galaxies: active – galaxies: evolution – galaxies: high-redshift – galaxies: nuclei – radio continuum: galaxies.

1 INTRODUCTION

The search for high-redshift radio galaxies has been somewhat overshadowed in recent years by the discovery of significant numbers of radio-quiet quasars from the Sloan Digital Sky Survey (e.g. Fan et al. 2003). However, the bright point-source nature of the quasars means that it is extremely difficult to study the stellar populations of the host galaxies of these powerful active galactic nuclei (AGN). For this reason alone it is still useful to search for distant radio galaxies.

Furthermore, there are extremely important roles that radio galaxies may play in our understanding of general galaxy formation and evolution. First, the fact that they are selected via radio emission means that they are essentially free of selection effects inherent to optical surveys, such as dust obscuration, which may be more prevalent in the early Universe (e.g. Archibald et al. 2001), and particularly around massive galaxies (Stevens et al. 2003). Secondly, in radio galaxies the powerful nuclear emission is obscured by the 'dusty torus' in orientation-based unification schemes; thus we have an uninhibited view of any neutral gas all the way up to the host galaxy, without the problem of the ionized Strömgren sphere along the line of sight from which quasars suffer. This means that the gas, which possibly helped in the formation of the galaxy and in fuelling the AGN, can be probed up to the vicinity of the host galaxy itself (e.g. Jarvis et al. 2003; Wilman et al. 2004). Thirdly, if we discover powerful radio galaxies within the epoch of reionization, we would be able to probe the 21-cm forest at this important epoch in the history of the Universe (e.g. Carilli, Gnedin & Owen 2002). Fourthly, it is also now known that powerful radio galaxies in the high-redshift Universe trace overdensities of galaxies (e.g. Venemans et al. 2002; Miley et al. 2004) which may go on to become the richest clusters in the nearby Universe and thus provide a probe of large-scale structure formation over all cosmic epochs. A fifth reason is that they are very luminous, allowing for detailed studies of cold, warm and hot gas using millimetre, optical and X-ray telescopes (e.g. Villar-Martín et al. 2003; Carilli 2003; Stevens et al. 2003).

In the past decade the search for radio galaxies at the highest redshifts has been optimized using various selection techniques. The

⋆E-mail: mjj@astro.ox.ac.uk

Report Documentation Page

Form Approved
OMB No. 0704-0188

1. REPORT DATE	2. REPORT TYPE	3. DATES COVERED
2004		**00-00-2004 to 00-00-2004**

4. TITLE AND SUBTITLE	5a. CONTRACT NUMBER
Near-infrared K-band imaging of a sample of ultra-steep-spectrum radio sources selected at 74 MHz	5b. GRANT NUMBER
	5c. PROGRAM ELEMENT NUMBER
6. AUTHOR(S)	5d. PROJECT NUMBER
	5e. TASK NUMBER
	5f. WORK UNIT NUMBER
7. PERFORMING ORGANIZATION NAME(S) AND ADDRESS(ES) **Naval Research Laboratory,Code 7213,4555 Overlook Avenue, SW,Washington,DC,20375**	8. PERFORMING ORGANIZATION REPORT NUMBER
9. SPONSORING/MONITORING AGENCY NAME(S) AND ADDRESS(ES)	10. SPONSOR/MONITOR'S ACRONYM(S)
	11. SPONSOR/MONITOR'S REPORT NUMBER(S)

12. DISTRIBUTION/AVAILABILITY STATEMENT
Approved for public release; distribution unlimited

13. SUPPLEMENTARY NOTES

14. ABSTRACT

15. SUBJECT TERMS

16. SECURITY CLASSIFICATION OF:			17. LIMITATION OF ABSTRACT	18. NUMBER OF PAGES	19a. NAME OF RESPONSIBLE PERSON
a. REPORT	b. ABSTRACT	c. THIS PAGE			
unclassified	**unclassified**	**unclassified**		**11**	

most widely used of these is that of a steep radio spectral index. This works because radio spectra are generally concave, and thus they steepen at high frequencies. This is particularly true at the highest redshifts, where the inverse Compton losses, due to the increase in temperature of the cosmic microwave background, are higher. Further, the observed rest-frame frequencies are higher for high-redshift sources. Therefore, by filtering a sample to include just those sources with steep spectral indices, one would expect to select in favour of high-redshift objects. This idea has in fact been verified by several groups (e.g. Blundell et al. 1998; De Breuck et al. 2000, 2001; Jarvis et al. 2001a,b).

Another important radio selection criterion is that of low frequency. This is because the spectra of the highest-redshift sources are redshifted towards low frequency; thus the bulk of the flux from the source itself, although emitted at higher frequencies, is observed at much lower frequencies, and this effect obviously increases with redshift. Thus the majority of surveys for high-redshift radio galaxies have taken place at frequencies $\ll$1 GHz, the two most prominent being 325 MHz (De Breuck et al. 2000, 2001) and 151 MHz (Blundell et al. 1998; Jarvis et al. 2001a,b), which have found the highest-redshift radio galaxies to date (Rawlings et al. 1996; van Breugel et al. 1999). Low-frequency selection also preferentially selects the optically thin lobe emission, which is independent of orientation, unlike high-frequency selection, which preferentially selects the optically thick emission from the core of the AGN, which means that low-frequency surveys are crucial for unification studies (e.g. Willott et al. 2000). The next step in this type of survey would be to push the observed frequency lower.

The new 74-MHz system on the Very Large Array (VLA), fully implemented in 1998 (Kassim et al. 1993), has opened up a new window into the previously unexplored regime of very low-frequency radio observations at high sensitivity and sub-arcminute resolution. Therefore, we have initiated a survey at this low frequency, with steep spectral index selection, to continue the search for the highest-redshift radio galaxies. The radio data for this survey are described in Cohen et al. (2004), and have $\sim$10 times the resolution and sensitivity of 8C. In this paper we present our near-infrared *K*-band follow-up observations of all the steep-spectrum sources in this sample.

This paper is set out as follows. In Section 2 we summarize how the sample was selected, and in Section 3 we describe the *K*-band observations, which are then presented in Section 4. In Section 5, we compare the distribution of *K*-band magnitude with similar samples selected at higher frequencies, and in Section 6 we discuss our results.

2 SAMPLE SELECTION

Full details of how the sample was selected can be found in Cohen et al. (2004). For clarity we summarize the selection criteria here.

(i) $S_{74\,\mathrm{MHz}} \geqslant 0.1$ Jy. This is a lower limit, as the sensitivity is a function of position on the sky, due to areas of higher noise. We refer the reader to Cohen et al. (2004) for full details.

(ii) Spectral index between 74 and 1400 MHz, $\alpha_{74}^{1400} < -1.2$, where $S_\nu \propto \nu^\alpha$. The NRAO VLA Sky Survey (NVSS; Condon et al. 1998) was used to measure the 1400-MHz flux densities as the low angular resolution ($\sim$40 arcsec) is well matched to that of the 74-MHz observations ($\sim$25 arcsec); therefore we do not expect any extended structure to be resolved out in either survey.

This leads to a sample of 26 sources detected over a total area of 0.05 sr.

3 *K*-BAND IMAGING

3.1 Observations

The *K*-band (2.2 μm) imaging of the 74-MHz ultra-steep-spectrum (USS) sample was made over several flexibly scheduled runs at the United Kingdom Infrared Telescope (UKIRT), beginning in 2003 December up to 2004 March. The observations were made using the high-resolution infrared camera on UKIRT, UFTI (UKIRT Fast-Track Imager), which comprises a 1024 × 1024 HgCdTe array, with a plate scale of 0.091 arcsec pixel^{-1}, giving a field of view of 92 × 92 arcsec^2. All observations were made in photometric conditions, with seeing always <0.6 arcsec, with the tip-tilt system.

In order to subtract the rapidly changing sky background at these wavelengths, to provide a good flat-field and to minimize the effects of cosmic ray contamination and bad pixels, we used the standard observing strategy of offsetting the position of the telescope by $\sim$10 arcsec between each exposure. The offsets were arranged in a 3 × 3 mosaic of nine exposures. The integration time varies between objects in the sample, with the fainter sources being observed for longer. A summary of all the *K*-band observations is given in Table 1.

3.2 Data reduction

The *K*-band images were reduced using standard procedures. We first subtracted the dark current from each image. We then divided by the normalized flat-field, created by combining the nine exposures of the particular field with a median filter, which removes any objects that appear in different positions on the chip over the nine exposures. To combine the individual images we registered all of the frames using a bright star that was present in each of the nine pointings. In the cases where there was no bright star in the images, the offsets recorded in the image headers were used to align the frames. The registered images were then combined using an average clipping procedure to reject pixels more than 4σ away from the median of the distribution.

Astrometry for each image was achieved by identifying sources in the image with objects in the POSS-II. In all cases, apart from J1252.7+2207, we were able to identify three or more sources on our images with objects on the finding charts. In these cases the astrometry, performed with the KARMA-KOORDS task package[1] (Gooch 1996), which performs a simple linear fit to the plate solution, is typically (for UFTI) accurate to $\lesssim$1 arcsec. Photometric calibration was performed using at least two UKIRT faint standard stars on each night where data were taken. The reduced images are shown in Fig. 1 with the Faint Images of the Radio Sky at Twenty centimetres (FIRST; Becker, White & Helfand 1995) radio contours overlaid. The FIRST survey was carried out at 1.4 GHz and has an angular resolution of $\sim$5 arcsec.

4 RESULTS

In Table 2 we present the *K*-band magnitudes for all of the sources in our 74-MHz USS sample. The magnitudes have been measured in three apertures of 3, 5 and 8 arcsec respectively, both to allow ease of comparison with previous work and to make sure that a magnitude is given even when there is a nearby object that may increase the flux in one of the larger apertures.

[1] http://www.atnf.csiro.au/computing/software/karma/

Table 1. Log of the *K*-band imaging observations for our 74-MHz USS sample.

Source	Dates observed	Total exposure time (s)
J1225.0+2146	2004-02-12	2700
J1226.3+2418	2004-01-19	540
J1228.9+3114	2003-12-24, 2004-01-17, 2004-01-19, 2004-04-09	3240
J1229.1+3040	2003-12-24, 2004-01-17, 2004-01-19, 2004-02-12	3240
J1229.9+3712	2003-12-24, 2004-01-17	1080
J1230.2+2326	2004-01-19	540
J1230.6+3247	2003-12-24	540
J1231.2+2538	2004-01-19, 2004-02-13	1620
J1231.3+3724	2004-01-17	540
J1231.5+3236	2004-01-17	540
J1232.2+2814	2004-01-17, 2004-02-20	2160
J1232.6+3157	2004-02-13	1080
J1234.3+2605	2004-01-17	540
J1238.2+2613	2004-01-17	540
J1238.8+3559	2004-01-17	540
J1243.7+2830	2004-01-17	540
J1245.9+3320	2004-02-20	540
J1246.4+2516	2004-01-17, 2004-02-20	1620
J1248.2+2747	2004-01-17	540
J1249.0+3615	2004-01-19	540
J1249.7+3408	2004-02-20, 2004-02-27, 2004-04-07	5400
J1250.4+2941	2004-01-17	540
J1252.7+2207	2004-01-17	540
J1253.4+2703	2004-01-17	540
J1253.6+2509	2004-01-17	540
J1256.9+2811	2004-01-17, 2004-02-12	2160

4.1 Notes on individual sources

In this section we present notes on all of the individual sources in the 74-MHz USS sample. In the cases where there is an infrared counterpart within 1.5 arcsec (or within the positional uncertainty of the individual astrometrized images) of the core of a one-component radio source, or within 1.5 arcsec of the axis along a double-lobed source, we take this to be the true identification (ID) of the radio source host galaxy.

J1225.0+2146

This source is double-lobed, with an extended *K*-band ID towards the western lobe. There are two plausible candidates for the ID, which may be interacting, at $\alpha = 12{:}25{:}02.40$, $\delta = 21{:}46{:}52.6$ with $K = 20.12$, and $\alpha = 12{:}25{:}02.51$, $\delta = 21{:}46{:}54.5$ with $K = 20.20$. The entry in Table 2 is the magnitude for the westernmost ID. There is also a faint infrared source at the centre of the western lobe ($\alpha = 12{:}25{:}02.14$, $\delta = 21{:}46{:}50.6$), with a *K*-band magnitude $K > 21$; this is unlikely to be the ID but could be enhanced emission due to the passage of the radio jet.

J1226.3+2418

This is a large radio source with a secure ID at the centre of the brightest radio emission.

J1228.9+3114

This source has a slightly extended radio morphology centred at $\alpha = 12{:}28{:}59.58$, $\delta = +31{:}14{:}57.6$. There is a bright *K*-band counterpart to the north-east of this centroid at $\alpha = 12{:}28{:}59.56$, $\delta = +31{:}15{:}01.1$, which may be the host galaxy. However, this is not centred on the bright radio emission, and it is possible that a true ID centred on the radio emission may be beyond the detection limit of our imaging observations at $K > 20.7$ in a 3-arcsec aperture (3σ).

J1229.1+3040

This source is slightly extended in the radio map. We have a total of 3240 s integration with UKIRT on this source with no apparent ID down to a limiting 3σ total magnitude of $K = 20.7$ in a 3-arcsec aperture.

J1229.9+3712

The radio morphology for this source is such that it could be the lobe of a larger source. Indeed, inspection of the FIRST radio maps does show three aligned components with a probable core at $\alpha = 12{:}30{:}02.98$, $\delta = 37{:}12{:}46.1$. The full extent of this radio source on the sky is $\sim$3 arcmin. The FIRST radio map overplotted on the Digitized Sky Survey *R*-band image is shown in Fig. 2. There is no bright ID detected in the POSS-II image at the position of the core.

J1230.2+2326

This source has a double-lobed radio morphology with a bright *K*-band ID situated between them, along the radio axis.

J1230.6+3247

This is an extended radio source with two *K*-band counterparts close to both of the bright radio components. This could be two

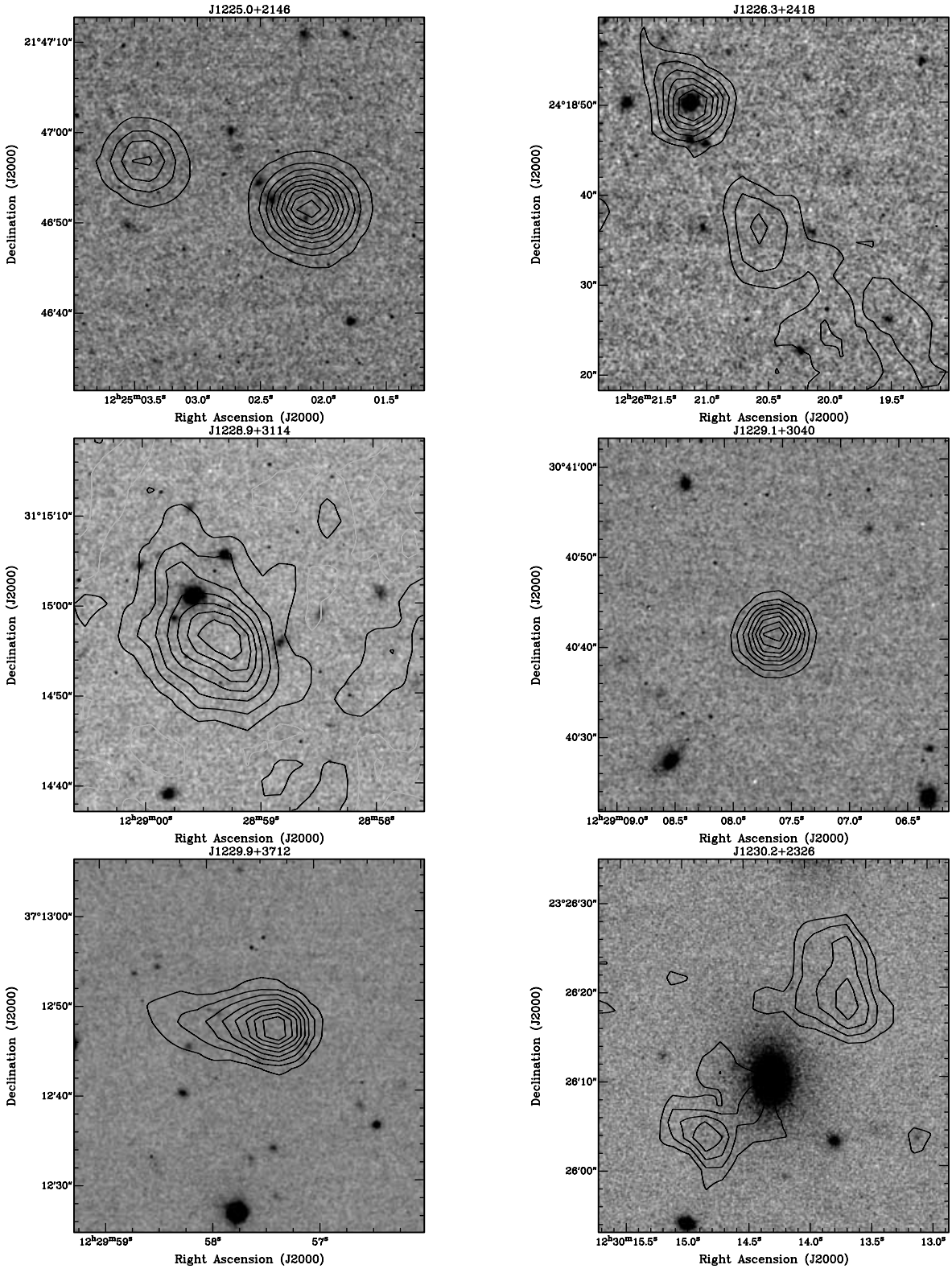

Figure 1. (a) The *K*-band images (grey-scale) of the 26 USS sources from our 74-MHz sample. The images have been smoothed for presentation purposes. The black contours represent the radio maps from the 1.4-GHz FIRST survey. The contour levels are incremented by 10 per cent of the peak flux density unless stated otherwise. J1225.0+2146, peak flux density = 23.05 mJy beam^{-1}, lowest contour is 10 per cent of the peak flux density. J1226.3+2418, peak flux density = 2.29 mJy beam^{-1}, lowest contour is 35 per cent of the peak. J1228.9+3114, peak flux density = 1.88 mJy beam^{-1}, lowest contour is 30 per cent of the peak. J1229.1+3040, peak flux density = 6.32 mJy beam^{-1}, lowest contour is 20 per cent of the peak. J1229.9+3712, peak flux density = 5.54 mJy beam^{-1}, lowest contour is 20 per cent of the peak. J1230.2+2326, peak flux density = 0.92 mJy beam^{-1}, lowest contour is 55 per cent of the peak with increments of 8 per cent.

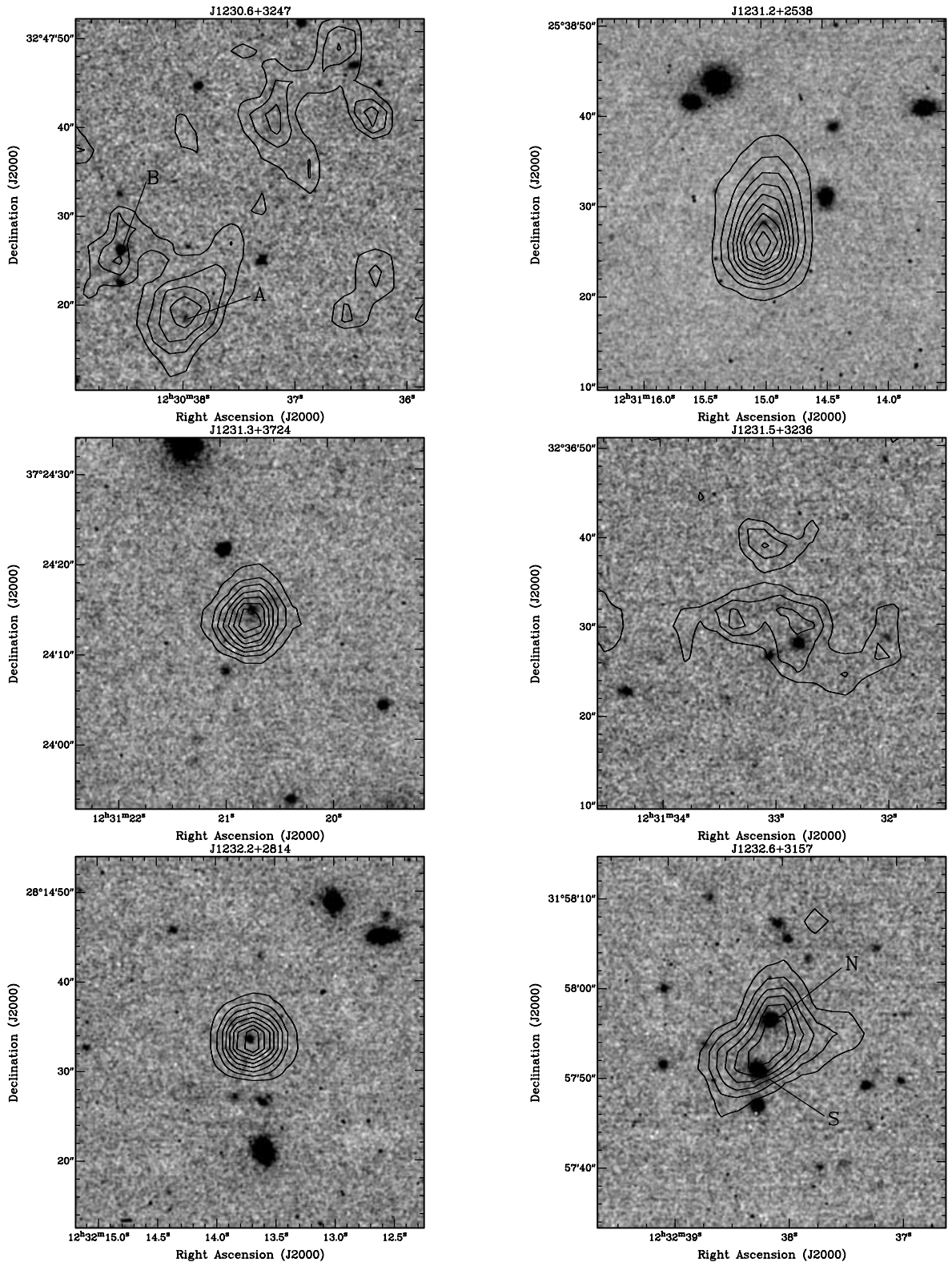

Figure 1. (b) Contour levels incremented by 10 per cent of peak flux density unless stated otherwise. J1230.6+3247, peak flux density = 0.59 mJy beam^{-1}, lowest contour is 60 per cent of the peak flux density with increments of 8 per cent. J1231.2+2538, peak flux density = 15.55 mJy beam^{-1}, lowest contour is 10 per cent of the peak. J1231.3+3724, peak flux density = 2.75 mJy beam^{-1}, lowest contour is 30 per cent of the peak. J1231.5+3236, peak flux density = 0.50 mJy beam^{-1}, lowest contour is 70 per cent of the peak with increments of 5 per cent. J1232.2+2814, peak flux density = 5.26 mJy beam^{-1}, lowest contour is 20 per cent of the peak. J1232.6+3157, peak flux density = 1.94 mJy beam^{-1}, lowest contour is 40 per cent of the peak.

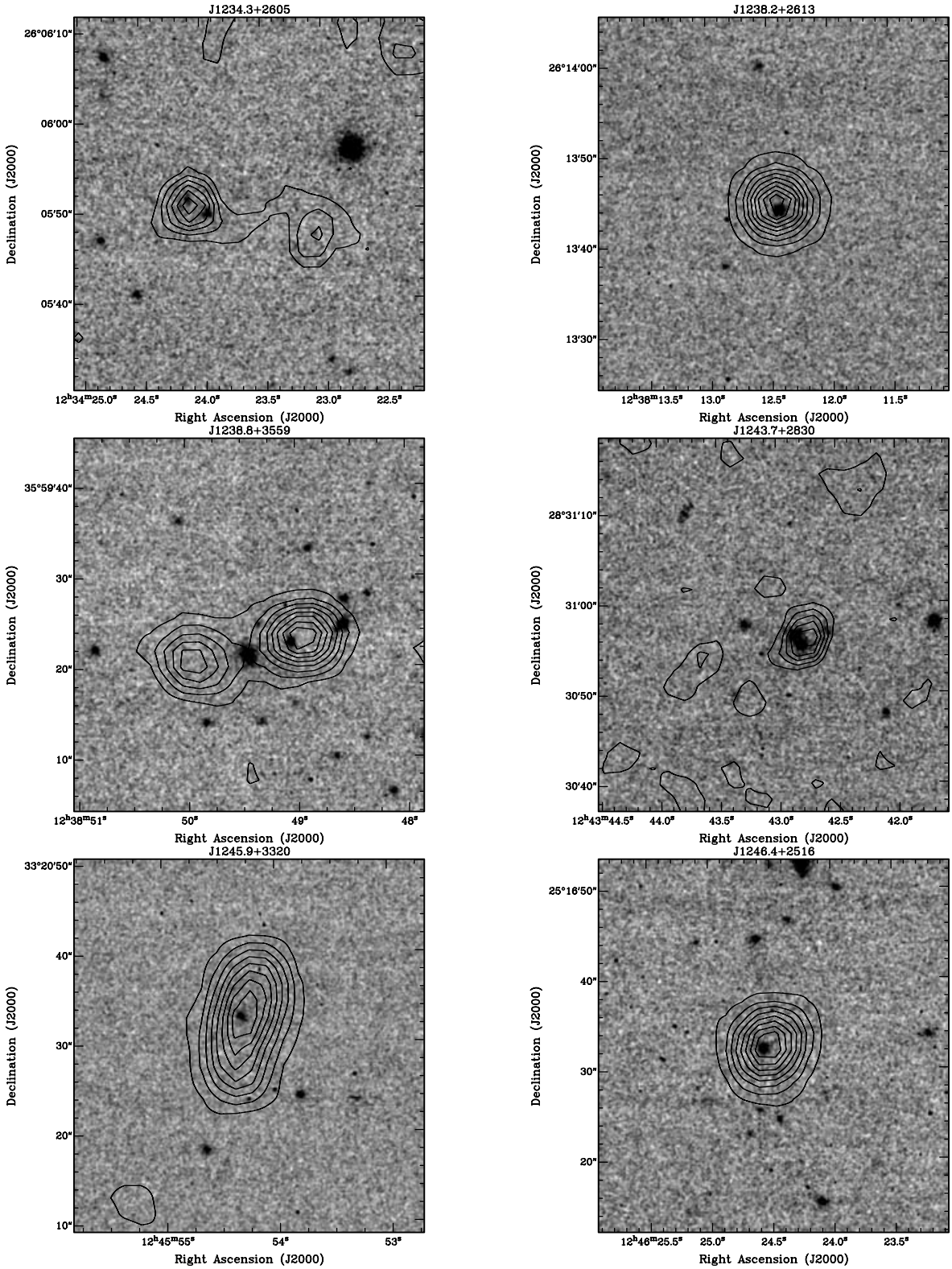

Figure 1. (c) Contour levels incremented by 10 per cent of peak flux density unless stated otherwise. J1234.3+2605, peak flux density = 1.73 mJy beam^{-1}, lowest contour is 40 per cent of the peak flux density. J1238.2+2613, peak flux density = 15.68 mJy beam^{-1}, lowest contour is 10 per cent of the peak. J1238.8+3559, peak flux density = 4.16 mJy beam^{-1}, lowest contour is 20 per cent of the peak. J1243.7+2830, peak flux density = 0.98 mJy beam^{-1}, lowest contour is 50 per cent of the peak with increments of 8 per cent. J1245.9+3320, peak flux density = 4.45 mJy beam^{-1}, lowest contour is 20 per cent of the peak. J1246.4+2516, peak flux density = 4.25 mJy beam^{-1}, lowest contour is 20 per cent of the peak.

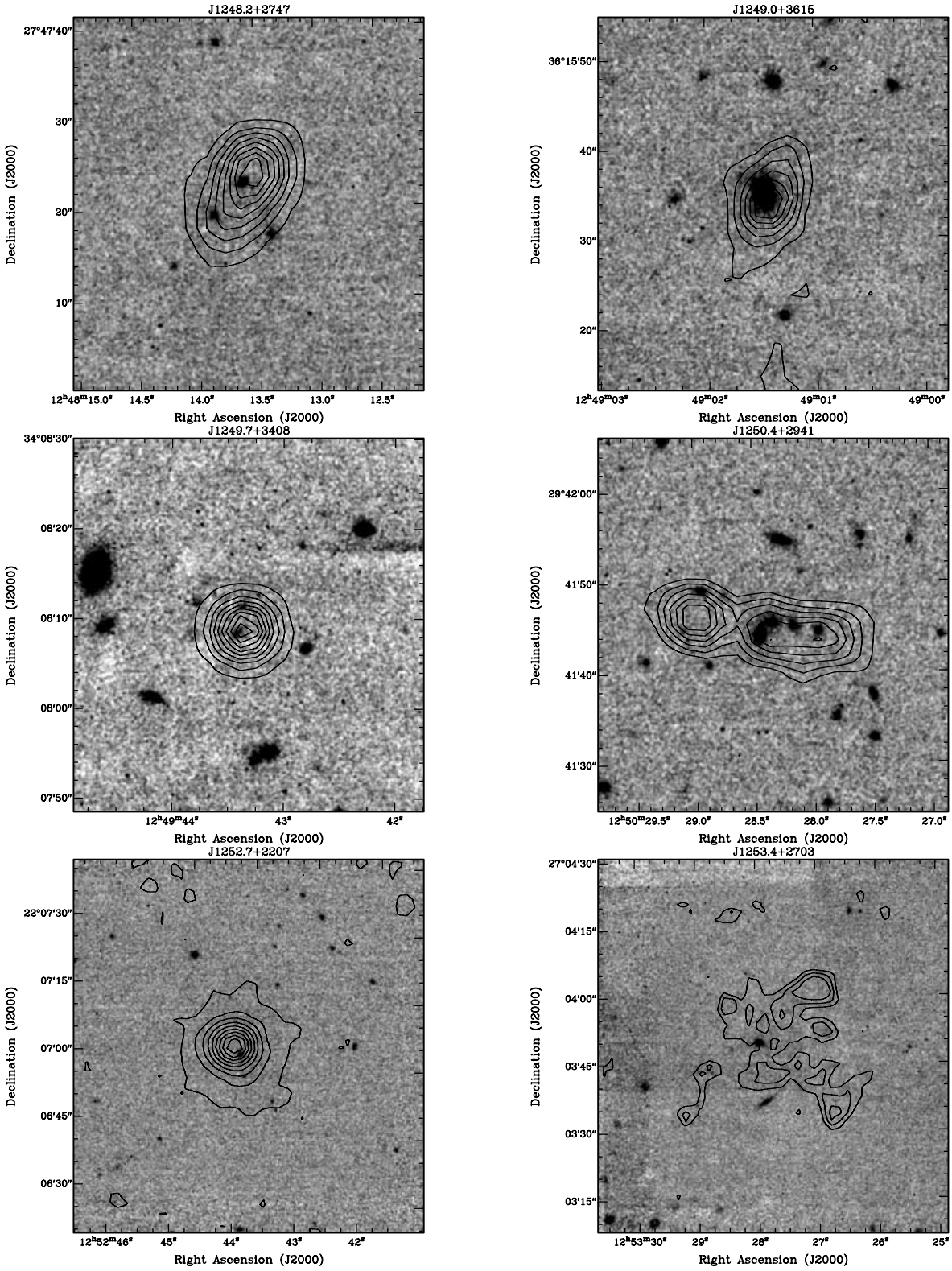

Figure 1. (d) Contour levels incremented by 10 per cent of peak flux density unless stated otherwise. J1248.2+2747, peak flux density = 4.34 mJy beam^{-1}, lowest contour is 20 per cent of the peak flux density. J1249.0+3615, peak flux density = 2.05 mJy beam^{-1}, lowest contour is 35 per cent of the peak. J1249.7+3408, peak flux density = 34.45 mJy beam^{-1}, lowest contour is 10 per cent of the peak. J1250.4+2941, peak flux density = 1.59 mJy beam^{-1}, lowest contour is 40 per cent of the peak. J1252.7+2207, peak flux density = 6.66 mJy beam^{-1}, lowest contour is 10 per cent of the peak. J1253.4+2703, peak flux density = 0.81 mJy beam^{-1}, lowest contour is 65 per cent of the peak with increments of 8 per cent.

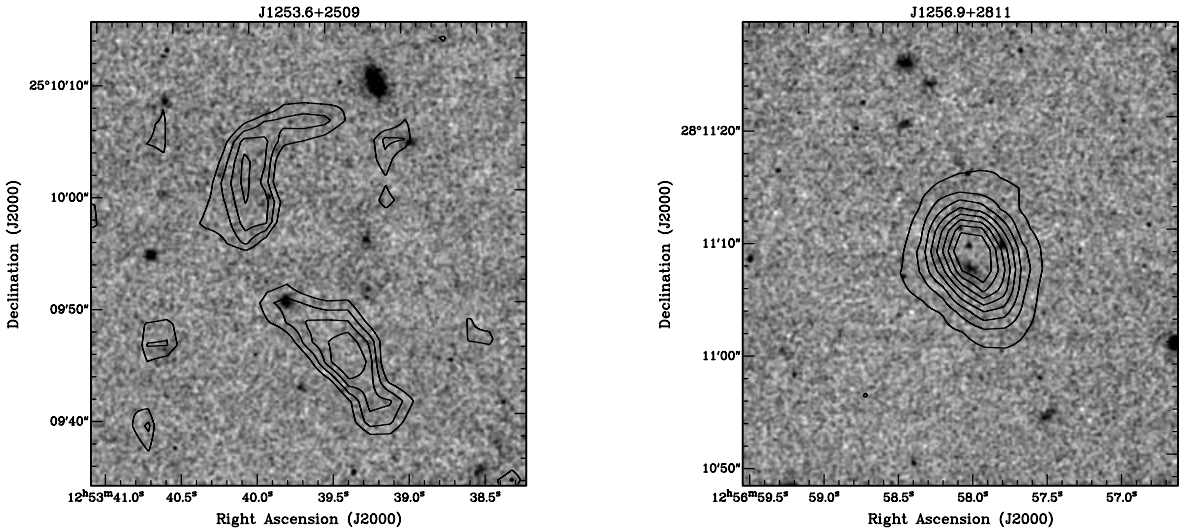

Figure 1. (e) Contour levels incremented by 10 per cent of peak flux density unless stated otherwise. J1253.6+2509, peak flux density = 0.55 mJy beam^{-1}, lowest contour is 70 per cent of the peak flux density with increments of 6 per cent. J1256.9+2509, peak flux density = 6.11 mJy beam^{-1}, lowest contour is 15 per cent of the peak.

Table 2. The *K*-band magnitudes for the 74-MHz USS sample in three different angular apertures. In columns 2–4, 'nbo' denotes that the radio galaxy is too close to a nearby object to measure the magnitude reliably. J1229.9+3712 is not shown as it is now omitted from the sample because the 74-MHz emission is from the lobe of a larger source (Fig. 2).

Source	Magnitude from 3-arcsec diameter	Magnitude from 5-arcsec diameter	Magnitude from 8-arcsec diameter	Notes
J1225.0+2146	20.12 ± 0.33	19.70 ± 0.32	19.54 ± 0.32	
J1226.3+2418	16.911 ± 0.087	16.764 ± 0.083	16.608 ± 0.080	
J1228.9+3114[a]	16.502 ± 0.079	16.276 ± 0.073	16.073 ± 0.069	
J1229.1+3040	>20.7	>20.2	>19.7	
J1230.2+2326	14.301 ± 0.026	13.922 ± 0.022	13.641 ± 0.019	
J1230.6+3247A	19.681 ± 0.375	19.675 ± 0.406	19.655 ± 0.502	ID on the western-most radio source
J1230.6+3247B	17.979 ± 0.151	17.911 ± 0.156	17.512 ± 0.140	ID on the radio source to the NE
J1231.2+2538	19.187 ± 0.225	18.780 ± 0.195	18.759 ± 0.225	
J1231.3+3724	18.098 ± 0.170	17.870 ± 0.161	17.814 ± 0.177	
J1231.5+3236	17.499 ± 0.128	17.276 ± 0.119	nbo	
J1232.2+2814	19.313 ± 0.266	19.363 ± 0.292	–	
J1232.6+3157N	17.512 ± 0.110	17.296 ± 0.101	17.151 ± 0.097	North source
J1232.6+3157S	17.376 ± 0.103	17.159 ± 0.094	16.726 ± 0.078	South source
J1234.3+2605	18.585 ± 0.218	17.992 ± 0.173	17.786 ± 0.176	
J1238.2+2613	17.543 ± 0.130	17.521 ± 0.134	17.662 ± 0.162	
J1238.8+3559	16.961 ± 0.099	16.724 ± 0.091	16.522 ± 0.087	
J1243.7+2830	17.255 ± 0.113	16.996 ± 0.103	16.717 ± 0.096	Merger?
J1245.9+3320	18.405 ± 0.178	18.082 ± 0.162	17.695 ± 0.151	
J1246.4+2516	18.552 ± 0.187	18.507 ± 0.192	18.516 ± 0.223	
J1248.2+2747	17.672 ± 0.139	17.508 ± 0.134	17.413 ± 0.143	
J1249.0+3615	15.862 ± 0.054	15.607 ± 0.048	15.500 ± 0.047	Merger?
J1249.7+3408	20.093 ± 0.396	19.576 ± 0.320	19.483 ± 0.340	
J1250.4+2941	16.815 ± 0.092	nbo	nbo	
J1252.7+2207	17.856 ± 0.151	17.624 ± 0.142	17.447 ± 0.145	
J1253.4+2703	16.777 ± 0.090	16.592 ± 0.085	16.511 ± 0.087	
J1253.6+2509	18.674 ± 0.230	18.628 ± 0.258	18.503 ± 0.322	
J1256.9+2811	19.466 ± 0.288	19.224 ± 0.272	18.885 ± 0.257	

[a]The quoted magnitudes are for the bright galaxy to the north-east; the actual ID may not be visible in this image (see notes on this source).

distinct sources with both of the two infrared objects hosting an AGN (marked A and B in Fig. 1). We note that the peak centroid of the 74-MHz radio map is centred closer to the south-western component with the fainter *K*-band ID at α = 12:30:37.96, δ = +32:47:18.2 (referred to as J1230.6+3247A), and we consider this to be the most likely near-infrared counterpart.

J1231.2+2538

This is a compact radio structure with a faint *K*-band ID at its centre.

J1231.3+3724

This is a compact radio source with a faint *K*-band ID at its centre.

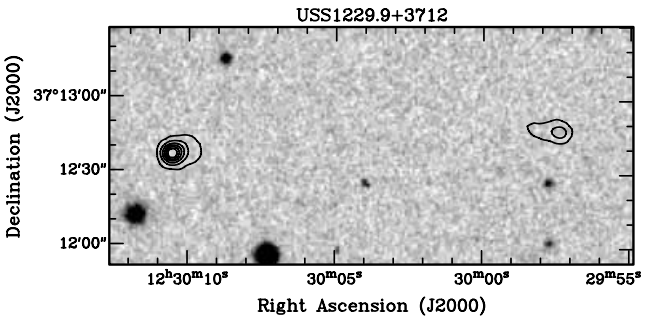

Figure 2. POSS-II *R*-band image of J1229.9+3712. The contours represent the FIRST source, which is almost certainly a large source extending to ∼3 arcmin. The 74-MHz USS source is situated at the position of the western lobe. The peak flux density of the radio emission is 18.60 mJy beam^{-1}, and the lowest contour is at 8 per cent of this value, with increments of 15 per cent.

J1231.5+3236

This source has a very extended radio morphology with a *K*-band ID at its centre. There also seems to be an overdensity of radio sources close to the radio source, possibly indicative of a cluster.

J1232.2+2814

This is another compact radio source with a faint *K*-band ID at its centre.

J1232.6+3157

This is a small but extended radio morphology with two bright *K*-band counterparts towards each of the extended components. This could be a superposition of two sources or one radio source with two plausible IDs, or alternatively it could be lensed. Spectroscopy will be needed to distinguish between these possibilities. The *K*-band magnitudes of both the northern object (J1232.6+3157N) and southern object (J1232.6+3157S) are given in Tables 2 and 3. Given the similarity in *K*-band magnitude, the distribution in *K*-band magnitude of this sample is not affected significantly by choosing one counterpart over the other for this radio source.

J1234.3+2605

This is a double-lobed radio source with a plausible *K*-band ID towards the eastern lobe. There is also a fainter *K*-band source at the centre of the eastern lobe at $\alpha = 12{:}34{:}24.12$, $\delta = 26{:}05{:}51.4$. Both are within 1.5 arcsec of the centre of the radio lobe and either could be the ID. We assume for this paper that the brighter source is the ID, as it lies along the radio axis.

J1238.2+2613

This is a compact radio source with a *K*-band ID at its centre.

Table 3. Summary of the key observational results for the 74-MHz USS sample. The quoted RA and Dec. are for the positions of the *K*-band IDs and all are J2000. The quoted lower limit for J1229.1+3040 is the 3σ limit in an 8-arcsec aperture.

Source	RA (^{h} ^{m} ^{s}.)	Dec. ($^\circ$ $'$ $''$.)	74-MHz flux density (Jy)	α_{74}^{1400}	*K* mag (8 arcsec)
J1225.0+2146	12 25 02.40	+21 46 52.6	2.213	−1.25	19.54 ± 0.32
J1226.3+2418	12 26 21.11	+24 18 50.3	0.943	−1.36	16.608 ± 0.080
J1228.9+3114[a]	12 28 59.56	+31 15 01.1	0.608	−1.36	16.073 ± 0.069
J1229.1+3040	12 29 07.75	+30 40 41.2	0.356	−1.27	>19.7
J1229.9+3712[b]	12 30 02.98	+37 12 46.1	0.635	−1.25	
J1230.2+2326	12 30 14.31	+23 26 14.5	0.968	−1.63	13.641 ± 0.019
J1230.6+3247A[c]	12 30 37.96	+32 47 18.2	0.188	< −1.4	19.655 ± 0.502
J1231.2+2538	12 31 15.00	+25 38 28.0	1.064	−1.20	18.759 ± 0.225
J1231.3+3724	12 31 20.71	+37 24 14.7	0.477	−1.51	17.814 ± 0.177
J1231.5+3236	12 31 32.78	+32 36 28.1	0.311	−1.52	17.276 ± 0.119[d]
J1232.2+2814	12 32 13.71	+28 14 33.8	0.327	−1.36	19.363 ± 0.292[d]
J1232.6+3157N	12 32 38.13	+31 57 56.2	0.359	−1.35	17.151 ± 0.097
J1232.6+3157S	12 32 38.25	+31 57 50.7	0.359	−1.35	16.726 ± 0.078
J1234.3+2605	12 34 23.95	+26 05 49.7	0.402	−1.61	17.786 ± 0.176
J1238.2+2613	12 38 12.42	+26 13 44.0	0.728	−1.30	17.662 ± 0.162
J1238.8+3559	12 38 49.44	+35 59 21.4	0.634	−1.33	16.522± 0.087
J1243.7+2830	12 43 42.80	+28 30 55.5	0.712	−1.73	16.717 ± 0.096
J1245.9+3320	12 45 54.30	+33 20 33.0	1.140	−1.40	17.695 ± 0.151
J1246.4+2516	12 46 24.55	+25 16 32.4	0.347	−1.29	18.516 ± 0.223
J1248.2+2747	12 48 13.62	+27 47 22.8	0.624	−1.31	17.413 ± 0.143
J1249.0+3615	12 49 01.46	+36 15 34.4	0.440	−1.20	15.500 ± 0.047
J1249.7+3408	12 49 43.43	+34 08 08.5	1.383	−1.23	19.483 ± 0.340
J1250.4+2941	12 50 28.45	+29 41 44.2	0.395	−1.35	16.815 ± 0.092[e]
J1252.7+2207	12 52 44.04	+22 07 01.5	0.940	−1.22	17.447 ± 0.145
J1253.4+2703	12 53 27.96	+27 03 49.9	0.838	−1.30	16.511 ± 0.087
J1253.6+2509	12 53 39.78	+25 09 50.5	0.472	< −1.7	18.503 ± 0.322
J1256.9+2811	12 56 58.15	+28 11 09.7	0.524	−1.32	18.885 ± 0.257

Notes. [a]The quoted magnitudes are for the bright galaxy to the north-east; the actual ID may not be visible in this image (see notes on this source). [b]This is a large source where the 74-MHz ID is associated with an extended lobe (Fig. 2). [c]The quoted magnitude relates to the *K*-band ID at J1230.6+3247A. [d]The *K*-band magnitudes are measured using a 5-arcsec diameter aperture. [e]Measured in a 3-arcsec apertures, given due to the proximity of a *K*-band source to the ID.

J1238.8+3559

This is a double-lobed radio source with a bright *K*-band source at the centre of the radio structure, which we take to be the ID. There are also two further *K*-band sources stretching along the western lobe, which could be due to jet-induced star formation, although spectroscopy will be needed to confirm that these objects are at the same redshift as the radio source.

J1243.7+2830

This is a compact radio structure with a *K*-band ID at its centre. There is also another *K*-band source of similar magnitude that may be interacting with this central galaxy ∼1.3 arcsec to the north-east.

J1245.9+3320

This is a slightly extended radio source with a faint *K*-band ID at its centre.

J1246.4+2516

This is a compact radio source with a faint *K*-band ID in the centre.

J1248.2+2747

This source has a slightly extended radio morphology with a fairly bright *K*-band ID close to (∼1 arcsec away from) the centre.

J1249.0+3615

This is an extended radio source with a bright *K*-band ID at the centre of the brightest point in the radio emission, which we take to be the core. This galaxy has a very close possible companion ∼1 arcsec to the north with which it may be interacting. The 74 MHz centroid for this source is ∼12 arcsec to the north of the core position quoted here. This may be because the 74-MHz emission arises from a more extended, optically thin lobe.

J1249.7+3408

This is a compact radio source with a very faint *K*-band ID at the centre. There are also three fainter sources in the immediate vicinity (<6 arcsec away) of the ID, which may be associated with an overdensity of galaxies at high redshift (the *K*-band magnitude of this source means that it is likely to be at $z > 4$).

J1250.4+2941

This source is a highly extended double-lobed radio source in the east–west direction. There is a bright ID at the centre of the source, with a line of three fainter sources aligned along the western lobe. This is highly unlikely to be a chance alignment, and therefore these three sources may be due to gas compression by the jet causing increased star formation, or could be due to a preferred orientation of galaxy overdensities with respect to the jet axis. Spectroscopy will be needed to confirm whether these are actually at the same redshift as the radio source.

J1252.7+2207

This is a fairly compact source with a *K*-band ID near its centre. The astrometry on this image is only good to ∼1.5 arcsec; therefore it is very plausible that the ID is actually at the centre of the radio centroid.

J1253.4+2703

This source has a very unusual morphology in the radio, and in Cohen et al. (2004) we suggested that it could be a cluster relic. There is a bright *K*-band source near the centre of the radio emission, but spectroscopy will be needed to confirm whether this is associated with the radio emission.

J1253.6+2509

This is a double-lobed radio source with a *K*-band ID centred on the northernmost extent of the southern lobe, along the axis of the radio emission.

J1256.9+2811

This is a compact source with a very faint *K*-band ID consistent with being at its centre.

5 COMPARISON WITH OTHER SAMPLES

In this section we compare the distributions of *K*-band magnitude of the USS sample with the distribution of magnitudes from a similar survey selected at 151 MHz and also with a steep-spectrum filtering criterion, namely 6C* (Jarvis et al. 2001a,b). The *K*-band magnitudes can be used to estimate the redshift of a source given the observed tightness of the *K*–*z* relation (e.g. Jarvis et al. 2001a; Willott et al. 2003). Fig. 3 shows the histogram of the *K*-band magnitudes for the USS sample and the 6C* sample.

A Kolmogorov–Smirnov test shows that the two data sets are consistent with being drawn from the same underlying distribution, with the probability that they are drawn from different distributions significant at $<2\sigma$. However, Fig. 3 does show that there are more bright near-infrared sources in the 74-MHz-selected USS sample. This is predominantly due to the fact that the 6C* sample has an angular size limit of 15 arcsec, which may effectively filter out closer objects, which are not excluded from the 74-MHz sample.

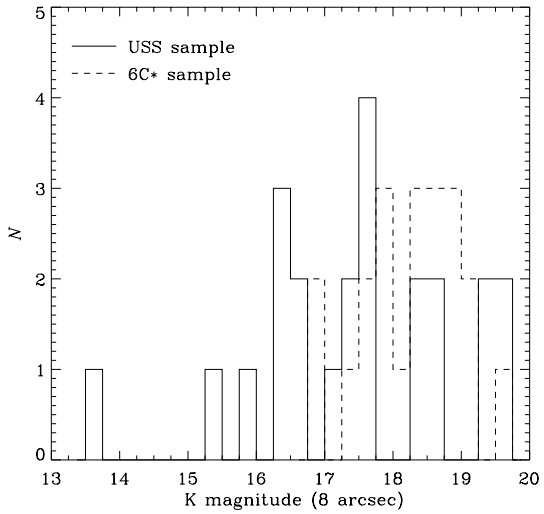

Figure 3. Histogram of the *K*-band magnitudes of the 74-MHz USS sample (solid line) and the 151-MHz selected 6C* sample (dashed line).

Indeed, of those sources with $K < 17$, four of them have angular sizes >15 arcsec. Removing these sources from the distribution results in the distribution in the K-band magnitudes for the 74-MHz USS and 6C* samples being completely indistinguishable, with the probability that they were drawn from the same underlying distribution >99 per cent ($>5\sigma$).

Given that the 6C* sample has a median redshift of $z \sim 1.9$ (Jarvis et al. 2001b), then we would expect that the USS sample discussed in this paper would have a similar redshift distribution, based on the K-band magnitudes. This is a much higher median redshift than unfiltered, complete surveys of similar flux density limit, such as 7CRS, where the median redshift is $z \sim 1.1$ (Willott et al. 2002). Therefore, we are confident that the USS technique is still viable at 74 MHz, and as such we envisage that this sample will contain some of the highest-redshift radio galaxies found to date.

6 SUMMARY

We have completed K-band imaging of a complete sample of 74-MHz USS sources selected from a region spanning 165 deg^2. This sample has been filtered using the steep spectral index criterion to target the highest-redshift radio galaxies. We find that the distribution in the K-band magnitudes is similar to that from a similar survey (6C*) undertaken at the slightly higher frequency of 151 MHz.

However, the 74-MHz USS sample is relatively overabundant in brighter sources when compared with the 6C* sample. This is predominantly due to the angular size cut-off used for the 6C* sample, which is not used for the 74-MHz USS sample here. Using this selection criterion on the 74-MHz USS sample would remove this bright near-infrared magnitude tail, and the probability that the two samples are drawn from the same underlying distribution is significant at >99 per cent.

The faint tail of the K-band magnitude distribution implies that we are still sensitive to the highest-redshift radio galaxies, with our faintest source having $K > 20.7$ (3-arcsec aperture), suggesting a redshift of $z > 5$ if we extrapolate the K–z relation for radio galaxies to $z > 5$.

The next stage in this project will be to gain spectroscopic redshifts of all of the sources in the sample, which will enable us to find some of the highest-redshift radio galaxies and also constrain the evolution in the comoving space density of the radio source population.

ACKNOWLEDGMENTS

MJJ acknowledges the support of a PPARC PDRA. MJC acknowledges the support from the Portuguese Fundação para a Ciência e a Tecnologia. The United Kingdom Infrared Telescope is operated by the Joint Astronomy Centre on behalf of the UK Particle Physics and Astronomy Research Council. Basic research in radio astronomy at the Naval Research Laboratory is supported by the Office of Naval Research. The National Radio Astronomy Observatory is a facility of the National Science Foundation operated under cooperative agreement by Associated Universities Inc. The Digitized Sky Surveys were produced at the Space Telescope Science Institute under US Government grant NAG W-2166. The images of these surveys are based on photographic data obtained using the Oschin Schmidt Telescope on Palomar Mountain and the UK Schmidt Telescope. The plates were processed into the present compressed digital form with the permission of these institutions. The Second Palomar Observatory Sky Survey (POSS-II) was made by the California Institute of Technology with funds from the National Science Foundation, the National Geographic Society, the Sloan Foundation, the Samuel Oschin Foundation, and the Eastman Kodak Corporation.

REFERENCES

Archibald E. N., Dunlop J. S., Hughes D. H., Rawlings S., Eales S. A., Ivison R. J., 2001, MNRAS, 323, 417
Becker R. H., White R. L., Helfand D. J., 1995, ApJ, 450, 559
Blundell K. M., Rawlings S., Eales S. A., Taylor G. B., Bradley A. D., 1998, MNRAS, 295, 265
Carilli C. L., 2003, New Astron. Rev., 47, 231
Carilli C. L., Gnedin N. Y., Owen F., 2002, ApJ, 577, 22
Cohen A. S., Röttgering H. J. A., Jarvis M. J., Kassim N. E., Lazio T. J. W., 2004, ApJS, 150, 417
Condon J. J., Cotton W. D., Greisen E. W., Yin Q. F., Perley R. A., Taylor G. B., Broderick J. J., 1998, AJ, 115, 1693
De Breuck C., van Breugel W., Röttgering H. J. A., Miley G., 2000, A&AS, 143, 303
De Breuck C. et al., 2001, AJ, 121, 1241
Fan X. et al., 2003, AJ, 125, 1649
Gooch R. E., 1996, PASA, 14, 106
Jarvis M. J. et al., 2001a, MNRAS, 326, 1563
Jarvis M. J., Rawlings S., Eales S. A., Blundell K. M., Bunker A. J., Croft S., McLure R. J., Willott C. J., 2001b, MNRAS, 326, 1585
Jarvis M. J., Wilman R. J., Röttgering H. J. A., Binette L., 2003, MNRAS, 338, 263
Kassim N. E., Perley R. A., Erickson W. C., Dwarakanath K. S., 1993, AJ, 106, 2218
Miley G. K. et al., 2004, Nat, 427, 47
Rawlings S., Lacy M., Blundell K. M., Eales S. A., Bunker A. J., Garrington S. T., 1996, Nat, 383, 502
Stevens J. A. et al., 2003, Nat, 425, 264
van Breugel W., De Breuck C., Stanford S. A., Stern D., Röttgering H. J. A., Miley G. K., 1999, ApJ, 518, 61
Venemans B. et al., 2002, ApJ, 569, 11
Villar-Martín M., Vernet J., di Serego Alighieri S., Fosbury R., Humphrey A., Pentericci L., 2003, MNRAS, 346, 271
Willott C. J., Rawlings S., Blundell K. M., Lacy M., 2000, MNRAS, 316, 449
Willott C. J., Rawlings S., Blundell K. M., Lacy M., Hill G. J., Scott S. E., 2002, MNRAS, 335, 1120
Willott C. J., Rawlings S., Jarvis M. J., Blundell K. M., 2003, MNRAS, 339, 173
Wilman R. J., Jarvis M. J., Röttgering H. J. A., Binette L., 2004, MNRAS, 351, 1109

This paper has been typeset from a TEX/LATEX file prepared by the author.